Cellular Physiology and Biochemistry

Cell Physiol Biochem 2017;42:1431-1446
DOI: 10.1159/000479207
Published online: July 17, 2017
Accepted: April 13, 2017

Original Paper

Effect of microRNA-135a on Cell Proliferation, Migration, Invasion, Apoptosis and Tumor Angiogenesis Through the IGF-1/PI3K/Akt Signaling Pathway in Non-Small Cell Lung Cancer

Yufei Zhou[a] Shaoxia Li[b] Jiangtao Li[c] Dongfeng Wang[a] Quanxing Li[a]

[a]Department of thoracic surgery, [b]Department of Pediatrics, The People's Hospital of Dongying, Dongying, [c]Department of General surgery, The second people's Hospital of Laiyang, Yantai, China

Key Words
microRNA-135a • Insulin-like growth factor-1 • IGF-1/PI3K/Akt signaling pathway • Non-small cell lung cancer • Proliferation • Migration • Invasion • Angiogenesis

Abstract
Objective: This study explored the ability of microRNA-135a (miR-135a) to influence cell proliferation, migration, invasion, apoptosis and tumor angiogenesis through the IGF-1/PI3K/Akt signaling pathway in non-small cell lung cancer (NSCLC). ***Methods:*** NSCLC tissues and adjacent normal tissues were collected from 138 NSCLC patients. Quantitative real-time polymerase chain reaction (qRT-PCR) was used to detect the expression levels of miR-135a and IGF-1, PI3K, Akt, VEGF, bFGF and IL-8 mRNA; western blotting was used to determine the expression levels of IGF-1, PI3K and Akt protein; and enzyme-linked immunosorbent assay (ELISA) was used to analyze the expression levels of VEGF, bFGF and IL-8 protein. Human NSCLC cell lines (A549, H460, and H1299) and the human bronchial epithelial cell line (HBE) were selected. A549 cells were assigned to blank, negative control (NC), miR-135a mimics, miR-135a inhibitors, IGF-1 siRNA and miR-135a inhibitors + IGF-1 siRNA groups. The following were performed: an MTT assay to assess cell proliferation, a scratch test to detect cell migration, a Transwell assay to measure cell invasion, and a flow cytometry to analyze cell apoptosis. ***Results:*** The expression level of miR-135a was lower while those of IGF-1, PI3K and Akt mRNA were higher in NSCLC tissues than in the adjacent normal tissues. Dual-luciferase reporter assay indicated IGF-1 as a target of miR-135a. The *in vitro* results showed that compared with the blank group, cell proliferation, migration and invasion were suppressed, mRNA and protein levels of IGF-1, PI3K, Akt, VEGF, bFGF and IL-8 were reduced, and cell apoptosis was enhanced in the miR-135a mimics and IGF-1 siRNA groups. Compared with the IGF-1 siRNA group, cells in the miR-135a inhibitors + IGF-1 siRNA group demonstrated increased cell proliferation, migration and invasion, elevated mRNA and protein levels of IGF-1, PI3K, Akt, VEGF, bFGF and IL-8 and reduced cell apoptosis. ***Conclusion:*** These findings indicated that miR-135a promotes

Dr. Yufei Zhou
Department of Thoracic Surgery, The People's Hospital of Dongying, 317# Nanyi Road, Dongying 257091 (China)
Tel. +86-0546-8331577, E-Mail zhouyufei22@163.com

cell apoptosis and inhibits cell proliferation, migration, invasion and tumor angiogenesis by targeting IGF-1 gene through the IGF-1/PI3K/Akt signaling pathway in NSCLC.

Introduction

Approximately 1.5 million individuals died of lung cancer worldwide in 2010, accounting for 19% of cancer deaths that year [1]. Statistics from the International Agency for Research on Cancer (IARC) showed that in 2008, there were approximately 520,000 new diagnoses of lung cancer in China, and non-small cell lung cancer (NSCLC) accounted for 85% of these [2, 3]. The incidence and mortality rates of NSCLC are the highest in developed countries and lowest in developing countries, but the number of deaths worldwide continues to rise [4]. Patients in early stages of NSCLC have a five-year survival rate of 40-67%. Unfortunately, more than 65% of NSCLC patients are diagnosed at advanced stages when potential interventions have little influence on prognosis [5-7]. Although a modest benefit is achieved by cytotoxic chemotherapy for patients with advanced NSCLC, the response rate is merely 20% to 35%, and patients exhibit a median survival ranging from 10 to 12 months [8]. Therefore, the underlying mechanisms of cell death in NSCLC should be explored to give rise to new therapeutic strategies. Recently, the involvement of microRNAs (miRNAs) in the biology and therapy of lung cancer has been a topic of intense research [9, 10].

miRNAs, a group of small, non-coding RNAs 21 to 25 nucleotides in length, can post-transcriptionally modulate gene expression by binding to complementary sequences in the 3' untranslated region (3' UTR) of the target messenger RNA, eventually resulting in the suppression of translation and reduction of protein expression [11]. Among the miRNAs, miRNA-135a (miR-135a) has been identified as a putative tumor suppressive miRNA, and its expression has been found to be reduced in several human cancers, such as gall bladder cancer and prostate cancer [12, 13]. An *in vitro* study also reported that miR-135a inhibited the migration and invasion of gastric cancer cells by targeting JAK2 [14]. With regards to the role of miR-135a in NSCLC, Zhang et al. found that the expression of miR-135a was reduced in the sera of NSCLC patients and was related to poor prognosis [15]. Additionally, it has been reported that the overexpression or restoration of miR-135a represses proliferation and facilitates apoptosis of tumor cells by its target genes c-Myc in renal cell carcinoma [16], JAK2 in lymphoma [17], and ROCK1 in gastric cancer [18]. We find that the PI3K/Akt signaling pathway is commonly investigated for its promotion of NSCLC progression *in vivo* and *in vitro* as the underlying mechanism of miR-135a in NSCLC [19, 20]. Interestingly, the findings of Ma et al. and Salani et al. provoked us to speculate that the IGF-1/PI3K/Akt signaling pathway may play an important role in NSCLC [21, 22]. Thereby, the aim of this study is to explore the ability of miR-135a to influence cell proliferation, migration, invasion, apoptosis and tumor angiogenesis through the IGF-1/PI3K/Akt signaling pathway in NSCLC.

Materials and Methods

Study subjects and specimen collection

NSCLC tissues were collected from 138 NSCLC patients admitted to our hospital between February 2013 and February 2016. The patients consisted of 106 males and 32 females, aged 38 to 72 years, with a mean age of 61.4 ± 10.2 years. They were diagnosed with NSCLC by a pathologist, and none of them received any anticancer therapies, such as radiotherapy, chemotherapy or molecular targeted therapy, before surgery. None of these patients had any acute or chronic diseases or other malignancies, and their clinical data were available for collection (Table 1). The patients were histologically classified according to Histological Typing of Lung and Pleural Tumors, Third Edition, issued by the World Health Organization (WHO) in 1999 [23]. The Seventh Edition of the Tumor, Node, Metastasis (TNM) Classification issued by the International Staging Committee (ISC) of the International Association for the Study of Lung Cancer

(IASLC) was used to evaluate the patients [24]. Corresponding adjacent normal tissues (more than 5 cm away from the lesion) from the patients were also collected as controls. A part of each specimen was rinsed with normal saline and stored in liquid nitrogen for further detection and analysis. Another part was fixed in neutral buffered formalin (NBF) for 24 h and embedded in paraffin. The protocol was approved by the Ethics Committee of our hospital, and written informed consent was obtained from each subject.

Table 1. Clinicopathological characteristics of 138 NSCLC patients. NSCLC, non-small cell lung cancer; SCC, squamous cell carcinoma; ASqC, adenosquamous carcinoma; TNM, tumor node metastasis; LNM, lymph node metastasis

Clinicopathological characteristics	Case	Ratio (%)
Age (year)		
< 60	80	58
≥ 60	58	42
Gender		
Male	106	76.8
Female	32	23.2
Histological type		
Adenocarcinoma	55	39.8
SCC	72	52.2
ASqC	11	8
TNM staging		
I + II	77	55.8
III	61	44.2
LNM		
Yes	35	25.4
No	103	74.6
Degree of differentiation		
High/moderate differentiation	97	70.3
Poor differentiation	41	29.7

Immunohistochemistry (IHC)

Paraffin-embedded sections (4 μm) were heated at 70°C for 15 min, dehydrated with an ethanol gradient, inactivated with H_2O_2, washed three times with phosphate buffer saline (PBS) (5 min/wash), blocked in goat serum at room temperature for 15 min, and incubated with 20~30 μL of PBS-diluted antibodies against IGF-1 (1:150), PI3K (1:300), Akt (1:200) and CD34 (ready-to-use). All antibodies were purchased from Zhongshan Golden Bridge Biotech Co., Beijing, China. The slides were incubated with PBS instead of primary antibody for the negative control. After incubation at 4°C overnight, the slices were washed three times with PBS, incubated in biotin-labeled secondary antibody (ready-to-use) at 37°C for 20 min, washed again with PBS, incubated in horseradish peroxidase (HRP)-labeled streptavidin at 37°C for 20 min, washed again with PBS, stained with diaminobenzidine (DAB) for 3~5 min and counterstained with hematoxylin for 5 min. Eventually, the slides were dehydrated, subjected to dimethylbenzene treatment, sealed with neutral gum and observed under a microscope.

The tumor area was identified under the microscope at 100× magnification. The cytoplasm and membrane of IGF-1-, PI3K- and Akt-positive cells were stained brown. Five high-magnification fields (400×) were selected at random for each slide, and 100 cells were counted in each field. The slides were independently scored by two senior pathologists in a double-blinded fashion. The number of positive cells was graded as 0 (< 5%), 1 (6-25%), 2 (26-50%), 3 (51-75%), or 4 (> 75%), and the intensity of the stain was graded as 0 (no color), 1 (yellow), 2 (light brown), or 3 (brown). The two grades were added, and the specimens were assigned to four levels: 0-1 score (-), 2 scores (+), 3-4 scores (++), and more than 5 scores (+++). The sum of the number of (++) and (+++) cells divided by the total cell number was used to express the percentage representative of the rate of positive expression [25]. CD34-labeled microvessel density (MVD) was quantified based on the methods established by Weidner et al. [26]. All slides were scanned using a microscope equipped with 100× objective to identify the area with the highest density of microvessels. The microvessels were quantified in five high-power fields (400×), and the average value was obtained.

Cell culture

The normal bronchus endothelial HBE cells and NSCLC cell lines (A549: lung adenocarcinoma cell lines that produce disaturated phosphatidylcholines to synthetize lecithin highly with unsaturated fatty acid, and the cytokeratin staining was positive; H460: human large cell lung cancer cell lines are established in the hydrothorax from a patient with large cell lung cancer; H1299: a cell line is derived from a lung cancer patient with lymph node metastasis and this patient received radiotherapy) were purchased from American Type Culture Collection (ATCC). All cells were routinely cultured in Dulbecco's modified Eagle's Medium (DMEM) (HyClone, Logan City, UT, USA) containing 10% fetal calf serum (FBS) and digested with trypsi (Gibco, Grand Island, NY, USA) in an incubator with 5% CO_2 at a constant temperature of 37°C. Cell digestion and passaging were performed at intervals of 2-3 days.

Cell grouping and transfection

A549 cells were assigned to the blank group (un-transfected A549 cells), miR-135a mimics group (cells transfected with miR-135a mimics), miR-135a inhibitors group (cells transfected with miR-135a inhibitors), negative control group (NC, cells transfected with non-sense sequence), IGF-1 siRNA group (cells transfected with IGF-1-specific siRNA) and miR-135a inhibitors + IGF-1 siRNA group (cells transfected with miR-135a inhibitors and IGF-1-specific siRNA). The oligonucleotides were purchased from GenePharma Co., Ltd. (Shanghai, China). A549 cells in the logarithmic growth phase were plated and cultured in antibiotic-free medium 24 h later. The medium was changed to serum-free Opti-MEM when the cell density reached 40%-60% of the plate. When the cell grew to 70% confluence, transfection was performed with Lipofectamine 2000 according to the manufacturer's instructions (11668-027, Invitrogen Inc., Carlsbad, CA, USA). The cells were mixed with transfection reagents and siRNA compounds (200 μl) and cultured in an incubator with 5% CO_2 at a constant temperature of 37°C for 6 h. After culture in serum-containing medium for 24-48 h, the cells were collected.

Dual-luciferase reporter assay

According to the online bioinformatics analysis software available at http://www.targetscan.org, a putative miR-135a binding site was predicted in the 3' UTR of IGF-1. According to the manufacturer's instructions (Promega, Madison, Wisconsin, USA), IGF-1 3' UTR-WT and IGF-1 3' UTR-MUT plasmids were constructed. DNA extraction was performed with the TIANamp Genomic DNA kit (Tiangen Biotechnology Co. Ltd, Beijing, China). Luciferase activity of the vectors was detected using a Dual-Luciferase Reporter Assay System (E1910, Promega, Madison, Wisconsin, USA). Forty eight hours after transfection, the medium was aspirated, and the DNA samples were rinsed twice with PBS and mixed with 100 μL of passive lysis buffer (PLB) at room temperature. Fifteen minutes later, the cell lysate was collected. After pre-reading for 2 s, 20 μL of Luciferase Assay Reagent II Stop & Glo® was added to 100 μL of each sample, and the bioluminescence value was read for 10 s.

MTT assay

After the transfected A549 cells reached 80% confluence, they were detached with trypsin and made into a single cell suspension. The cells were counted. The cells were seeded in 96-well plates with 3×10^3~6×10^3 cells in a volume of 200 μl in each well, and six replicate wells were prepared. The plates were cultured in an incubator with 5% CO_2 at 37°C for 24-72 h, and MTT solution was added to each well (5 mg/ml, Sigma-Aldrich, St Louis, MO, USA), followed by another 4 h of incubation in 5% CO_2 at 37°C. After the culture medium was aspirated, 150 μl of dimethyl sulfoxide (DMSO) was added to each well. Ten minutes later, the crystals were dissolved. Optical density (OD) of each well was measured at 12, 24, 48 and 72 h. MTT curves were plotted with OD values on the y-axis and time intervals on the x-axis. Each experiment was conducted three times.

Flow cytometry

Seventy-two hours after cell transfection, the cells were collected, washed three times with PBS, and resuspended in cold 500 μl 1 × binding buffer, mixed with 5 μl of Annexin-V-fluorescein isothiocyanate (FITC) and 2.5 μl of propidium iodide (PI), and eventually detected using a FACSAria Sorter (Becton Dickinson, San Jose, CA, USA). The scatter diagram was distributed as follows: Q4: healthy cells ($FITC^-/PI^-$); Q3: apoptotic cells at an early stage ($FITC^+/PI^-$); Q2: apoptotic cells at an advanced stage ($FITC^+/PI^+$). The apoptosis rate was calculated using the following equation: Apoptosis rate = ratio of apoptotic cells to the total cells in Q3 + ratio of apoptotic cells to the total cells in Q2. Each experiment was conducted three times.

Scratch test

Perpendicular and horizontal coordinates were outlined with intervals of 0.5-1.0 cm on the backs of 6-well plates. After cell transfection for 12-24 h, the A549 cells in logarithmic growth phase were plated in 6-well plates with the density of 5×10^5 cells/well. Once the cells grew to 80% confluence, a vertical scratch was made on the cell layer. The cells were incubated in McCoy's 5A medium with 5% CO_2 and saturated humidity at 37°C. The plates were photographed at 0, 24 and 48 h using an inverted microscope. Wound healing area was calculated using ImageTool (Bechtel Nevada, Los Alamos Operations) using the following formula: Wound healing rate = (initial scratch width - final scratch width) / initial scratch width × 100%.

Each experiment was conducted three times.

Transwell assay

Single cell suspensions at a density of 5×10^5 cells were prepared using serum-free medium. Matrigel at 4°C was diluted in serum-free DMEM at a ratio of 1:3. The diluted Matrigel (15 μl, 7.5 μl and 7.5 μl) was separately added into each upper chamber of Transwell plates (Corning, Inc., Corning, NY, USA) at 10 min intervals. Cell suspension (100 μl) was seeded in the upper chamber, while DMEM containing 0.5 ml 10% FBS was added to the lower chamber. The number of cells penetrating the Matrigel was used to assess the invasive ability of the cells. Each experiment was conducted three times.

Quantitative real-time polymerase chain reaction (qRT-PCR)

Total RNA isolation from the cells and tissues was performed using a TRIzol kit (TaKaRa Biotechnology Ltd., Dalian, China). The RNA samples were reversely transcribed into cDNA (10 μl) according to the manufacturer's instructions (DRR047S, TaKaRa Biotechnology Ltd., Dalian, China). The obtained cDNA was diluted in 65 μl of diethyl phosphorocyanidate (DEPC). The PCR mixture was prepared based on the following elements: 5 μl of SsoFast EvaGreen Supermix (1708882, Bio-Rad, Inc., Hercules, CA, USA), 0.5 μl of forward primer (10 μM), 0.5 μl of reverse primer (10 μM) and 4 μl of cDNA. The PCR conditions were as follows: pre-denaturation at 95°C for 1 min, 30 cycles of denaturation at 95°C for 30 s and annealing at 58°C for 5 s, followed by final extension at 72°C for 5 s. The primers were synthesized by Sangon Biological Engineering Technology & Services Co., Ltd. (Shanghai, China), and the sequences are listed in Table 2. With U6/GAPDH as the internal reference, three replicate wells were prepared for each sample and each gene. The validity of the PCR results was evaluated using melting curves. $\triangle Ct$ = CT (target gene) - CT (internal reference), $\triangle\triangle Ct$ = $\triangle Ct$ (experimental group) - $\triangle Ct$ (control group). The relative gene expression was quantified using the $2^{-\triangle\triangle Ct}$ method [27]. Each experiment was conducted three times.

Western blotting

Harvested A549 cells from the different groups were subjected to centrifugation and washed twice in PBS. Then, these cells were lysed on ice. Thirty minutes later, the cells were subjected to centrifugation (12000 ×g) at 4°C for 20 min, and the supernatant was stored at -20°C. With PBS, 2 μg/μl bovine serum albumin (BSA) was diluted to concentrations of 20 μg/ml, 15 μg/ml, 10 μg/ml, 5 μg/ml, 2.5 μg/ml and 0 μg/ml. According to bicinchoninic acid (BCA) detection kit's instructions (Thermo Fisher Scientific, San Jose, California, USA), the protein concentration was measured. The proteins were separated by 10% sodium dodecyl sulfate-polyacrylamide gel electrophoresis (SDS-PAGE) gels (80-120 V) and transferred onto polyvinylidene difluoride membranes (PVDF) (Millipore, Billerica, MA, USA). Then, the cells were blocked for 2 h at room temperature with 5% non-fat milk in Tris-buffered saline with Tween (TBST). The membranes were separately incubated at 4°C overnight in primary antibodies against IGF-1 (1:1000, ab106836), PI3K (1:1000, ab182651), AKT (1:500, ab8805) and GAPDH (1:1000, ab8245) (all primary antibodies were purchased from Abcam, Cambridge, MA, USA). Then, the membranes were washed three times using TBST (10 min for each wash), incubated in secondary antibodies at room temperature for 1 h, and washed three time again with TBST (10 min for each wash). Eventually, the membranes were subjected to chemiluminescence detection and exposed on X-ray films. The films were developed by photographic fixing, and the results were analyzed. Each experiment was conducted three times.

Enzyme-linked immunosorbent assay (ELISA)

The supernatant obtained from the cells was centrifuged to remove particulate matter and stored at -20°C to avoid repeated freezing and thawing. The expression levels of VEGF, bFGF and IL-8 were measured using ELISA according to the manufacturer's instructions (R&D Systems, Minneapolis, MN, USA). The blank group was set to zero, and the OD value of each well was measured at a wavelength of 450 nm using a microplate reader (Bio-Tek Instruments, Inc. Winooski, Vermont, USA).

Statistical analyses

SPSS software version 22.0 (SPSS Inc., Chicago, IL, USA) was used for statistical analyses. The data were expressed as the means ± standard deviation; *t*-test was performed for comparisons between two groups; one-way analysis of variance (ANOVA) was performed for comparisons among groups. Pearson correlation

analysis was conducted. *P*-values < 0.05 were accepted as significant differences.

Table 2. Primer sequences used for quantitative real-time polymerase chain reaction (qRT-PCR)

Gene	Sequences (5'-3')
miR-135a	Forward: 5'-TATGGCTTTTTATTCCTATGTGA-3'
	Reverse: 5'-TATGGCTTTTCATTCCTATGTGA-3'
U6	Forward: 5'-CTCGCTTCGGCAGCACA-3'
	Reverse: 5'-AACGCTTCACGAATTTGCGT-3'
IGF-1	Forward: 5'-AGGGTATGGCTCCAGCAGTC-3'
	Reverse: 5'-GAGGGGTGCGCAATACATCT-3'
PI3K	Forward: 5'-CGTTTCTGCTTTGGGACAAC-3'
	Reverse: 5'-CCTGATGATGGTCGTGGAG-3'
AKT	Forward: 5'-TGAGAGAAGCCACGCTGTC-3'
	Reverse: 5'-CGGAGAACAAACTGGATGAA-3'
VEGF	Forward: 5'-TAGACGTTCCCTGCCAGCAA-3'
	Reverse: 5'-AGCATCCGAGGAAAACATAAAATCTT-3'
bFGF	Forward: 5'-AAGAGCGACCCTCACATCAA-3'
	Reverse: 5'-TCGTTTCAGTGCCACATACC-3'
IL-8	Forward: 5'-GACATACTCCAAACCTTTCCACC-3'
	Reverse: 5'-AACCCTACAACAGACCCACA-3'
GAPDH	Forward: AACGGATTTGGTCGTATTGGG-3'
	Reverse: TCGCTCCTGGAAGATGGTGAT-3'

Results

The expression of miR-135a and expression levels of IGF-1, PI3K, Akt, VEGF, bFGF and IL-8 mRNA in NSCLC tissues and adjacent normal tissues

qRT-PCR was performed to detect the expression of miR-135a and expression levels of IGF-1, PI3K and Akt mRNA in NSCLC tissues and adjacent normal tissues. The results of qRT-PCR indicated that the expression of miR-135a was lower, while the expression levels of IGF-1, PI3K and Akt mRNA were higher in the NSCLC tissues than in the adjacent normal tissues ($P < 0.05$). The expression levels of VEGF, bFGF and IL-8 mRNA were also higher in the NSCLC tissues than in the adjacent normal tissues ($P < 0.05$). Pearson correlation analysis indicated that miR-135a expression was negatively correlated with the expression of IGF-1, PI3K and Akt mRNA (r = -0.890, $P < 0.001$; r = -0.946, $P < 0.001$; r = -0.938, $P < 0.001$, respectively) (Fig. 1).

Association between miR-135a expression and clinicopathological characteristics of NSCLC patients

Student's t-test was used to analyze the association between miR-135a expression and clinicopathological characteristics of NSCLC patients. As shown in Table 3, the expression of miR-135a was higher in the patients with stage I+II cancer than in those with stage III cancer ($P < 0.05$); the expression of miR-135a was lower in the patients with LNM than in those without ($P < 0.05$); the expression of miR-135a was higher in the highly/moderately differentiated tumors than in the poorly differentiated tumors ($P < 0.05$). The expression of miR-135a was not associated with age, gender or histological type ($P > 0.05$).

The expression of IGF-1, PI3K, Akt and CD34 protein in the NSCLC tissues and the adjacent normal tissues

IHC was used to assess the expression of IGF-1, PI3K, Akt and CD34 protein in NSCLC tissues and the adjacent normal tissues. IGF-1 protein was mainly localized in the cytoplasm (Fig. 2A). The positive staining for IGF-1 protein was higher in the NSCLC tissues (57.97%, 80/138) than in the adjacent normal tissues (26.81%, 37/138) ($P < 0.05$) (Fig. 2B). PI3K protein was mainly localized in the cytoplasm (Fig. 2C). The positive staining for PI3K protein was higher in the NSCLC tissues (51.45%, 71/138) than in the adjacent normal tissues (10.87%, 15/138) ($P < 0.05$) (Fig. 2D). Akt protein was mainly localized in the cytoplasm (Fig. 2E). The positive staining for Akt protein was higher in the NSCLC tissues (23.19%%, 32/138) than in the adjacent normal tissues (7.25%%, 9/138) ($P < 0.05$) (Fig. 2F). Although CD34 was expressed in both NSCLC tissues and adjacent normal tissues, CD34 was highly expressed in NSCLC tissues and labeled a number of vessels. Most of the vessels were intact, presenting as round shapes, round-like shapes and striped shapes (Fig. 2G). The NSCLC tissues (25.6 ± 7.3) exhibited higher CD34-MVD than the adjacent normal tissues (9.5 ± 4.9) ($P < 0.05$) (Fig. 2H, Table 4).

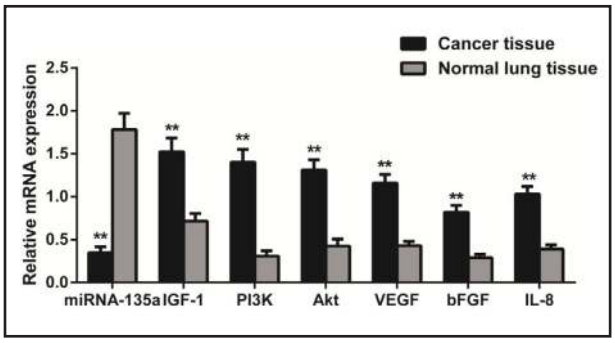

Fig. 1. The expression levels of miR-135a and IGF-1, PI3K, Akt, VEGF, bFGF and IL-8 mRNA in the NSCLC tissues and the adjacent normal tissues, detected by qRT-PCR. **, $P < 0.05$ compared with the adjacent normal tissues; miR-135a, microRNA-135a; IGF-1, insulin-like growth factor-1; PI3K, phosphatidylinositol 3-kinase; Akt, protein kinase B; qRT-PCR, quantitative real-time polymerase chain reaction.

Table 3. Association between clinicopathological characteristics of 138 NSCLC patients and the expression level of miR-135a. miR-135a, microRNA-135a; NSCLC, non-small cell lung cancer; SCC, squamous cell carcinoma; ASqC, adenosquamous carcinoma; TNM, tumor node metastasis; LNM, lymph node metastasis

Clinicopathological characteristics		Case	miR-135a	*P*
Age (year)				0.138
	< 60	80	0.355 ± 0.07	
	≥ 60	58	0.337 ± 0.07	
Gender				0.216
	Male	106	0.351 ± 0.07	
	Female	32	0.334 ± 0.06	
Histological type				0.066
	Adenocarcinoma	55	0.364 ± 0.07	
	SCC	72	0.337 ± 0.07	
	ASqC	11	0.329 ± 0.06	
TNM staging				0.032
	I + II	77	0.358 ± 0.07	
	III	61	0.332 ± 0.07	
LNM				0.021
	Yes	35	0.323 ± 0.04	
	No	103	0.356 ± 0.08	
Degree of differentiation				0.019
	High/moderate differentiation	97	0.351 ± 0.06	
	Poor differentiation	41	0.323 ± 0.07	

The expression of miR-135a and IGF-1 mRNA in human HBE cells and A549, H460 and H1299 cells

qRT-PCR was performed to determine the expression of miR-135a and IGF-1 mRNA in human HBE cells and A549, H460 and H1299 cells. Compared with the HBE cells, the expression of miR-135a was decreased while the expression of IGF-1 mRNA was increased in A549, H460 and H1299 cells ($P < 0.05$). Among these NSCLC cell lines, A549 cells exhibited the lowest level of miR-135a and the highest IGF-1 mRNA expression ($P < 0.05$) (Fig. 3). Therefore, the A549 cells were selected for further experimentation.

IGF-1 verified as a target of miR-135a

Target Scan software (http://www.targetscan. org/) was used to predict miR-135a binding sites on the 3' untranslated region (UTR) of IGF-1 mRNA. The binding site of miR-135a and the 3' UTR of IGF-1 are shown in Fig. 4A. Sequences of IGF-1 3' UTR with the binding site deleted and that of wild-type IGF-1 3' UTR were inserted into reporter plasmids. By detecting the luciferase activity in A549 cells that were co-transfected with miR-135a mimics and either Wt-miR-135a/IGF-1 or Mut-miR-135a/IGF-1, we found that the miR-135a mimics exerted no significant difference on the luciferase activity in the A549 cells transfected Wt-miR-135a/IGF-1, while the luciferase activity decreased approximately to 65% in the A549 cells transfected Mut-miR-135a/IGF-1 ($P < 0.05$, Fig. 4B).

Table 4. The expression of IGF-1, PI3K and AKT in the cancer tissue and adjacent normal tissue. IGF-1, insulin-like growth factor-1; PI3K, phosphatidylinositol 3-kinase; AKT, protein kinase B; CD34, human hematopoietic progenitor cell antigen; MVD, microvessel density

Protein	Cancer tissue	Adjacent normal tissue	*P*
IGF-1			
Positive case	80	37	< 0.001
Positive rate (%)	57.97	26.81	
PI3K			
Positive case	71	15	< 0.001
Positive rate (%)	51.45	10.87	
AKT			
Positive case	32	9	< 0.001
Positive rate (%)	23.19	7.25	
CD34			
MVD	25.6 ± 7.3	9.5 ± 4.9	< 0.001

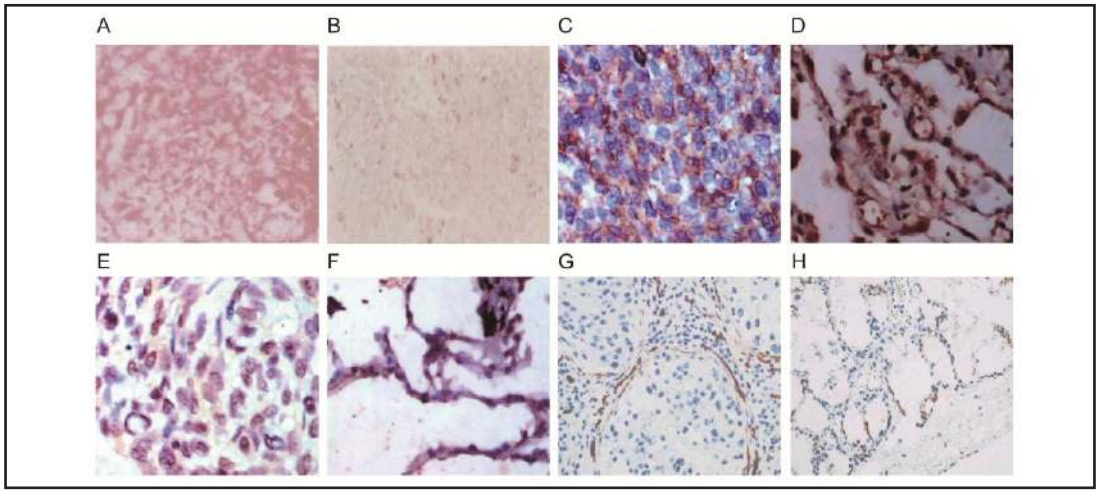

Fig. 2. The positive expression of IGF-1, PI3K, Akt and CD34 proteins in the NSCLC tissues and the negative expression of these proteins in the adjacent normal tissues, detected by IHC in (× 400). A, positive IGF-1 protein in the NSCLC tissues; B, negative IGF-1 protein in the adjacent normal tissues; C, positive PI3K protein in the NSCLC tissues; D, negative PI3K protein in the adjacent normal tissues; E, positive Akt protein in the NSCLC tissues; F, negative Akt protein in the adjacent normal tissues; G, positive CD34 protein in the NSCLC tissues; H, negative CD34 protein in the adjacent normal tissues; IGF-1, insulin-like growth factor-1; PI3K, phosphatidylinositol 3-kinase; Akt, protein kinase B; IHC, immunohistochemistry.

miR-135a suppressed proliferation of A549 cells by inhibiting IGF-1

MTT assay was used to evaluate proliferation of A549 cells. Twelve hours after transfection, there was no significant difference in proliferation among the six groups ($P > 0.05$). Twenty-four hours after transfection, compared with the blank group, cell proliferation was inhibited in the miR-135a mimics and IGF-1 siRNA groups but was promoted in the miR-135a inhibitors group ($P < 0.05$). There was no significant difference in proliferation among the NC, blank and miR-135a inhibitors + IGF-1 siRNA groups ($P > 0.05$). Compared with the IGF-1 siRNA group, cell proliferation was increased in the miR-135a inhibitors + IGF-1 siRNA group ($P < 0.05$) (Fig. 5). These results indicated that miR-135a suppressed proliferation of A549 cells by inhibiting IGF-1.

miR-135a promoted apoptosis of A549 cells by inhibiting IGF-1

Flow cytometry was used to evaluate apoptosis of A549 cells. Compared with the blank group, the apoptosis rate was increased in the miR-135a mimics and IGF-1 siRNA groups but was decreased in the miR-135a inhibitors group ($P < 0.05$). No significant difference was found in the apoptosis rate among the NC, blank and miR-135a inhibitors + IGF-1 siRNA groups ($P > 0.05$). Compared with the IGF-1 siRNA group, the apoptosis rate was reduced in

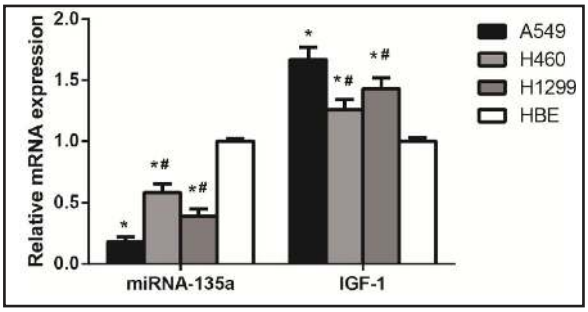

Fig. 3. The expression levels of miR-135a and IGF-1 mRNA in human HBE cells, A549, H460 and H1299 cells, detected by qRT-PCR. *, $P < 0.05$ compared with the HBE cells; #, $P < 0.05$ compared with the A549 cells; miR-135a, microRNA-135a; IGF-1, insulin-like growth factor-1; qRT-PCR, quantitative real-time polymerase chain reaction.

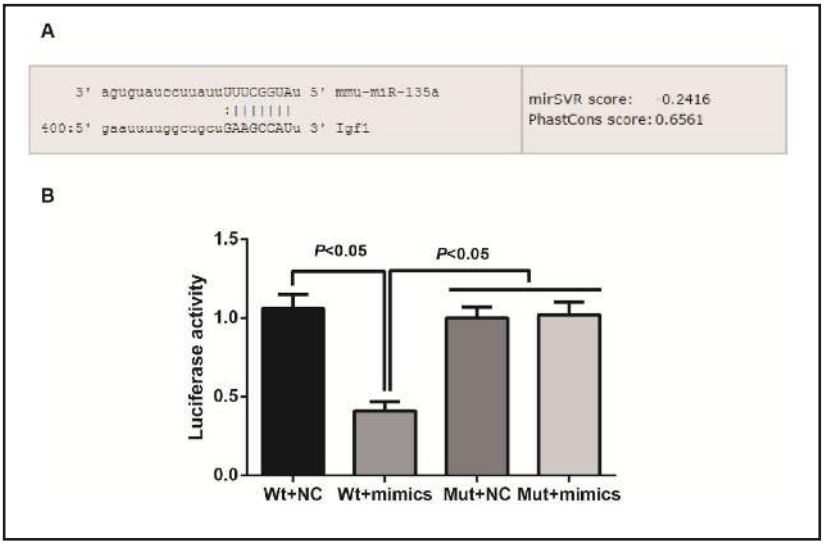

Fig. 4. IGF-1 verified as a target of miR-135a. A, Target Scan software was used to predict miR-135a with binding sites in the 3' untranslated region (UTR) of IGF-1 mRNA; B, detection of luciferase reporter gene activity: in the A549 cells cotransfected with miR-135a mimics and IGF-1 3'UTR Wt/Mut plasmids, miR-135a inhibited the luciferase activity of Wt plasmid but failed to affect the luciferase activity of Mut.

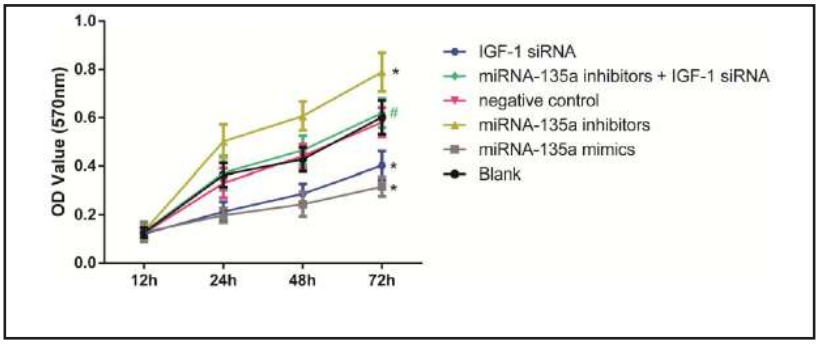

Fig. 5. The proliferation of A549 cells evaluated by MTT assay among blank, NC, miR-135a mimics, miR-135a inhibitors, IGF-1 siRNA and miR-135a inhibitors + IGF-1 siRNA groups. *, $P < 0.05$ compared with the blank group; #, $P < 0.05$ compared with the IGF-1 siRNA group.

the miR-135a inhibitors + IGF-1 siRNA group ($P < 0.05$) (Fig. 6). These data suggested that miR-135a promoted apoptosis in A549 cells by inhibiting IGF-1.

miR-135a suppressed migration of A549 cells by inhibiting IGF-1

Scratch assay was used to evaluate migration of A549 cells. In comparison with the blank group, cell migration was reduced in the miR-135a mimics and IGF-1 siRNA groups and was enhanced in the miR-135a inhibitors group ($P < 0.05$). No significant difference was found in cell migration among the NC, blank and miR-135a inhibitors + IGF-1 siRNA groups ($P > 0.05$). Compared with the IGF-1 siRNA group, cell migration was increased in the miR-135a inhibitors + IGF-1 siRNA group ($P < 0.05$) (Fig. 7). These data suggested that miR-135a suppressed migration of A549 cells by inhibiting IGF-1.

miR-135a suppressed invasion of A549 cells by inhibiting IGF-1

Transwell assay was used to evaluate invasion of A549 cells. Compared to the blank group, the miR-135a mimics and IGF-1 siRNA groups had lower numbers of cells penetrating

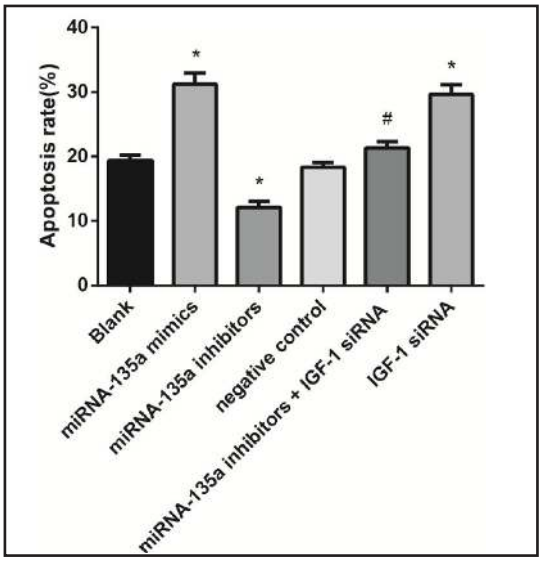

Fig. 6. The apoptosis of A549 cells evaluated by flow cytometry among the blank, NC, miR-135a mimics, miR-135a inhibitors, IGF-1 siRNA and miR-135a inhibitors + IGF-1 siRNA groups. *, $P < 0.05$ compared with the blank group; #, $P < 0.05$ compared with the IGF-1 siRNA group.

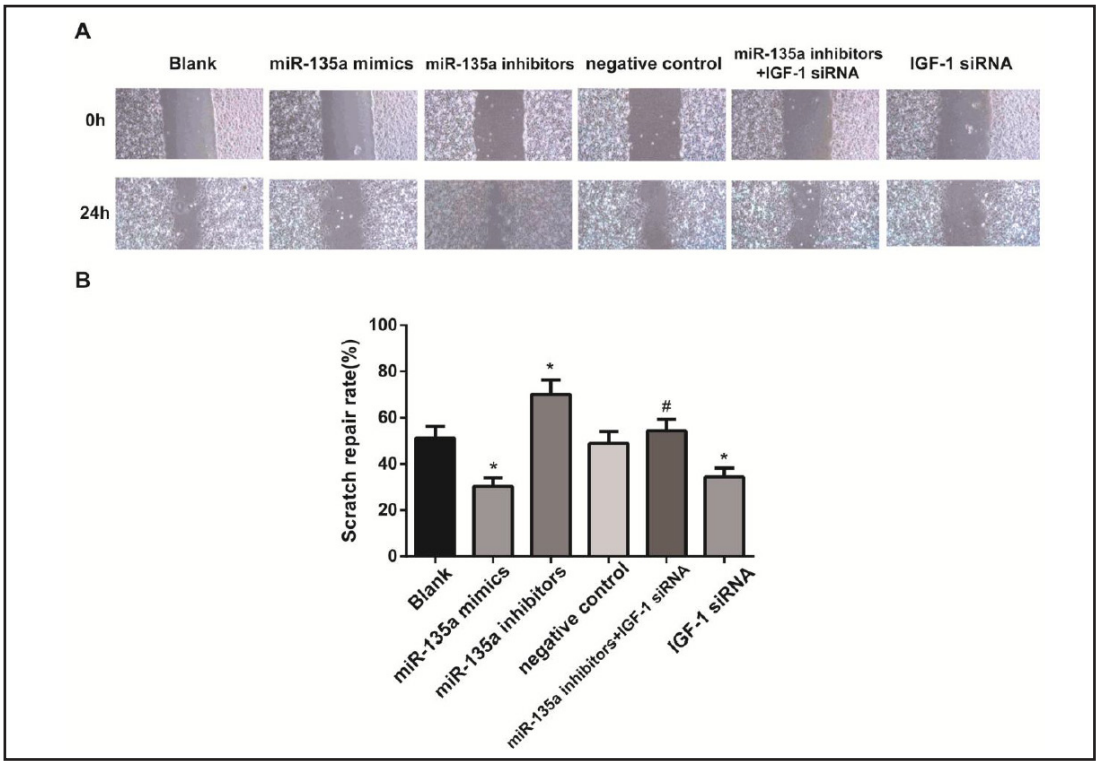

Fig. 7. The migration of A549 cells evaluated by scratch test among the blank, NC, miR-135a mimics, miR-135a inhibitors, IGF-1 siRNA and miR-135a inhibitors + IGF-1 siRNA groups. *, $P < 0.05$ compared with the blank group; #, $P < 0.05$ compared with the IGF-1 siRNA group.

into the matrix but the miR-135a inhibitors group had a higher number of cells penetrating into the matrix ($P < 0.05$). There was no significant difference in number of cells penetrating into the matrix among the NC, blank and miR-135a inhibitors + IGF-1 siRNA groups ($P > 0.05$). In comparison with the IGF-1 siRNA group, the miR-135a inhibitors + IGF-1 siRNA group had a number of cells penetrating into the matrix ($P < 0.05$) (Fig. 8). These data suggested that miR-135a suppressed invasion of A549 cells by inhibiting IGF-1.

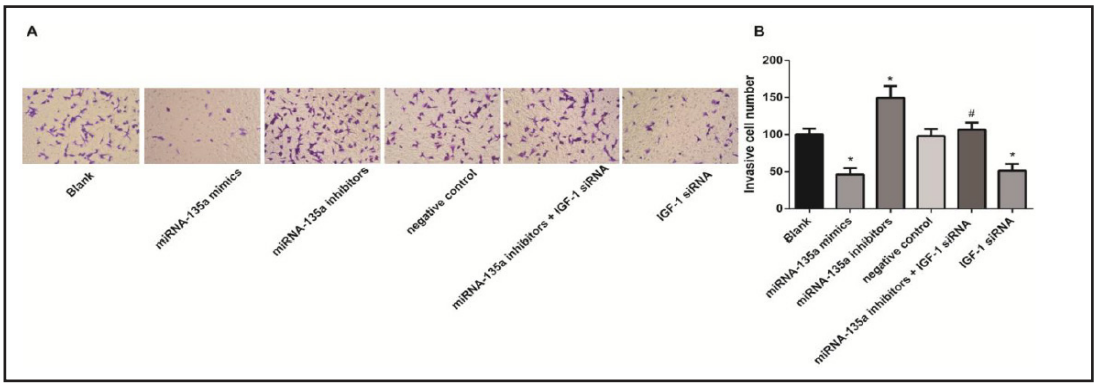

Fig. 8. The invasion of A549 cells evaluated by Transwell assay among the blank, NC, miR-135a mimics, miR-135a inhibitors, IGF-1 siRNA and miR-135a inhibitors + IGF-1 siRNA groups. A, cell invasion figures in each group; B, the number of cells penetrating into membrane in each group; *, $P < 0.05$ compared with the blank group; #, $P < 0.05$ compared with the IGF-1 siRNA group.

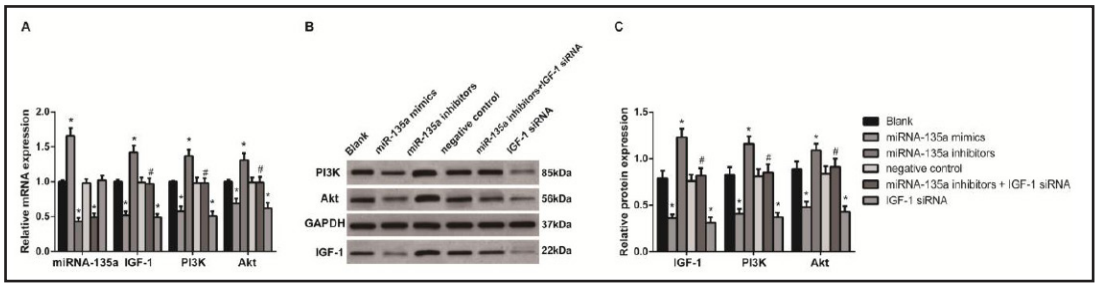

Fig. 9. The expression levels of IGF-1, PI3K and Akt mRNA and protein among the blank, NC, miR-135a mimics, miR-135a inhibitors, IGF-1 siRNA and miR-135a inhibitors + IGF-1 siRNA groups. A, the expression levels of miR-135a and IGF-1, PI3K and Akt mRNA; B, gray values of IGF-1, PI3K and Akt protein bands; C, the expression levels of IGF-1, PI3K and Akt protein; *, $P < 0.05$ compared with the blank group; #, $P < 0.05$ compared with the IGF-1 siRNA group; miR-135a, microRNA-135a; IGF-1, insulin-like growth factor-1; PI3K, phosphatidylinositol 3-kinase; Akt, protein kinase B; qRT-PCR, quantitative real-time polymerase chain reaction.

miR-135a blocked the IGF-1/PI3K/Akt signaling pathway in A549 cells

qRT-PCR and western blotting were used to detect the expression of miR-135a and the mRNA and protein levels of IGF-1, PI3K and Akt. Compared with the blank group, the expression of miR-135a was elevated in the miR-135a mimics group, while it was decreased in the miR-135a inhibitors and miR-135a inhibitors + IGF-1 siRNA groups ($P < 0.05$). No significant difference was detected among the NC, blank and IGF-1 siRNA groups ($P > 0.05$). In comparison with the blank group, the mRNA and protein levels of IGF-1, PI3K and Akt were reduced in the miR-135a mimics and IGF-1 siRNA groups but were enhanced in the miR-135a inhibitors group ($P < 0.05$). Compared to the IGF-1 siRNA group, the mRNA and protein levels of IGF-1, PI3K and Akt were elevated in the miR-135a inhibitors + IGF-1 siRNA group ($P < 0.05$) (Fig. 9). These findings revealed that miR-135a negatively targeted IGF-1 to block the IGF-1/PI3K/Akt signaling pathway.

miR-135a decreased angiogenesis-related factors VEGF, bFGF and IL-8 in A549 cells by inhibiting IGF-1

qRT-PCR and ELISA were used to determine the expression of VEGF, bFGF and IL-8 mRNA and protein. Compared to the blank group, the miR-135a mimics and IGF-1 siRNA groups exhibited lower VEGF, bFGF and IL-8 mRNA and protein levels while the miR-135a inhibitors group had higher VEGF, bFGF and IL-8 mRNA and protein levels ($P < 0.05$).

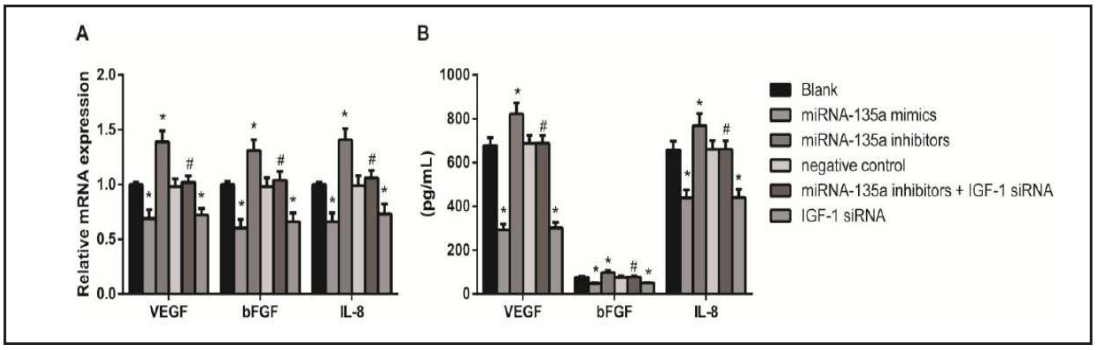

Fig. 10. The expression levels of VEGF, bFGF and IL-8 mRNA and protein among the blank, NC, miR-135a mimics, miR-135a inhibitors, IGF-1 siRNA and miR-135a inhibitors + IGF-1 siRNA groups. A, the expression levels of VEGF, bFGF and IL-8 mRNA; B, gray values of VEGF, bFGF and IL-8 protein bands; C, the expression levels of VEGF, bFGF and IL-8 protein; *, $P < 0.05$ compared with the blank group; #, $P < 0.05$ compared with the IGF-1 siRNA group; miR-135a, microRNA-135a; VEGF, vascular endothelial growth factor; bFGF, basic fibroblast growth factor; qRT-PCR, quantitative real-time polymerase chain reaction.

Compared with the IGF-1 siRNA group, the levels of VEGF, bFGF and IL-8 mRNA and protein were enhanced in the miR-135a inhibitors + IGF-1 siRNA group ($P < 0.05$) (Fig. 10). These results suggested that miR-135a decreased the expression of angiogenesis-related factors VEGF, bFGF and IL-8 in A549 cells by inhibiting IGF-1.

Discussion

As an emerging mechanism for the regulation of gene expression, miRNAs are considered critical regulators in the pathogenesis of cancer. miRNAs significantly affect various signaling pathways by modulating the expression of their target genes, thereby functioning as oncogenes or tumor suppressors [9]. In the present study, we explored the effects of miR-135a on cell proliferation, migration, invasion, apoptosis and tumor angiogenesis through the IGF-1/PI3K/Akt signaling pathway in NSCLC. Analysis of specimens collected from NSCLC patients and transfected cells *in vitro* demonstrated that miR-135a inhibits cell proliferation, migration, invasion and tumor angiogenesis and promotes cell apoptosis by targeting IGF-1 through the IGF-1/PI3K/Akt signaling pathway in NSCLC.

Importantly, our findings indicated that reduction in the expression of miR-135a was associated with the development and progression of NSCLC, and miR-135a inhibited proliferation, migration, invasion and promoted apoptosis of A549 cells by inhibiting the IGF-1/PI3K/Akt signaling pathway. miR-135a is encoded within 2 genes: MIRN135A1 and MIRN135A2, located at 3p21.1 and 12q23.1, respectively, and it has been proposed to suppress cancer progression. Consistent with our results, Zhang et al. found that the level of miR-135a was remarkably reduced in the sera of NSCLC patients compared to that of healthy control subjects and was associated with distant metastasis, LNM, TNM staging as well as the degree of differentiation of the tumors [15]. On the other hand, miR-135a has been demonstrated to have the capability of inducing apoptosis by directly targeting STAT6 [28]. STAT6 may mediate the expression of COX-2 to promote cancer development by increasing tumor invasion, resistance to apoptosis, and tumor angiogenesis [29]. In this study, we found that compared with the blank group, the A549 cells in the miR-135a mimics group has reduced proliferation, invasion and migration but higher rates of apoptosis; these findings were similar to the conclusions drawn by Shi et al. [30] who revealed that miR-135a restrained migration and invasion in NSCLC cells by acting on KLF-8. Additionally, miR-135a exhibits its tumor suppressive function by negatively regulating c-Myc, JAK2 and ROCK1 [16-18]. c-Myc is an oncogene that can enhance the aggressiveness of tumors and

is responsible for poor outcomes in NSCLC patients [31]. A significant positive correlation has been found between JAK2 activation and lung cancer grade. NSCLC patients with high levels of JAK2 exhibit a worse overall survival rate, and JAK2 activation promotes tumor angiogenesis in NSCLC cell lines *in vitro* [32]. In addition, the inhibition of ROCK1 is sufficient to block the growth and invasion of anchorage-independent NSCLC cells [33]. Additionally, as indicated in this study, miR-135a exerts its biological effect on A549 cells by inhibiting the IGF-1/PI3K/Akt signaling pathway. Fortunately, in our study, IGF-1 was confirmed as a well-established target gene of miR-135a, which is a novel discovery. As reflected in our study, the expression of IGF-1 was higher in the NSCLC tissues than in the adjacent normal tissues. Consistent with our results, Kim et al. reported that patients with low levels of IGF-1 have longer overall survival than those with high levels of IGF-1 and that IGF-1 overexpression predicts poor survival of NSCLC patients [34]. IGF-1 can bind to IGF-1R, thereby promoting growth, invasion and differentiation of lung cancer cells in an autocrine and/or paracrine manner [35]. Similarly, in our study, the A549 cells in the IGF-1 siRNA group had reduced proliferation, migration and invasion but increased apoptosis. The insulin-like growth factor (IGF) axis is an important growth-regulatory pathway that is prevalent in a variety of cancer types, including NSCLC [36]. It has been reported that IGF-1 plays an important role in the activation of the IGF-1/PI3K/Akt signaling pathway [37]. Our study found that compared with the A549 cells in the IGF-1 siRNA group, while those in the miR-135a inhibitors + IGF-1 siRNA group had higher proliferation, invasion, and migration as well as reduced apoptosis, which suggested that miR-135a resulted in the inhibition of the IGF-1/PI3K/Akt signaling pathway to suppress NSCLC cells.

In addition, one of the findings of this study implied that miR-135a inhibited tumor angiogenesis by inhibiting the IGF-1/PI3K/Akt signaling pathway. VEGF is an endothelial cell mitogen as well as a permeability factor that is highly angiogenic *in vivo* [38]. bFGF is an active polypeptide that is characterized by mitogenic, neurotrophic and angiogenic properties and as a proangiogenic factor in cancer occurrence and progression [39]. Also, Additionally, IL-8 is considered an angiogenic factor that is produced by endothelial cells, alveolar macrophages as well as monocytes [40]. In our *in vitro* experiments, the A549 cells in the miR-135a mimics group showed decreased expression levels of VEGF, bFGF and IL-8 compared to the cells in the blank group, indicating that miR-135a could inhibit tumor angiogenesis in NSCLC cells. Additionally, the study demonstrated that the cells in the IGF-1 siRNA group had reduced expression of VEGF, bFGF and IL-8 in comparison with the blank group. Li et al. have reported IGF-1-induced lung cancer angiogenesis [41], and Ma et al. have revealed that the inhibition of the PI3K/Akt/VEGF signaling pathway by PTEN may suppress tumor angiogenesis in human pancreatic cancer cells [42]. These findings, coupled with our results, potentially demonstrate that suppression of the IGF-1/PI3K/Akt signaling pathway exerts a significant inhibitory influence on tumor angiogenesis in NSCLC.

In conclusion, our study provided evidence that the inhibition of IGF-1/PI3K/Akt signaling pathway by miR-135a inhibits cell proliferation, migration, invasion and tumor angiogenesis and facilitates cell apoptosis in NSCLC. Our study is the first to explore the mechanism underlying the biological function of miR-135a, especially in tumor angiogenesis of NSCLC. Based on these findings, we concluded that miR-135a and IGF-1 may be considered as promising targets in new therapeutic approaches for inhibiting NSCLC progression and metastasis. Nevertheless, the conclusion should be strengthened by further studies with an established human NSCLC cell xenograft model to investigate the role of miR-135a and IGF-1 on tumor angiogenesis *in vivo*.

Acknowledgements

This work was not supported by any foundation

Disclosure Statement

The authors declare no conflict of interest.

References

1 Lozano R, Naghavi M, Foreman K, Lim S, Shibuya K, Aboyans V, Abraham J, Adair T, Aggarwal R, Ahn SY, Alvarado M, Anderson HR, Anderson LM, Andrews KG, Atkinson C, Baddour LM, Barker-Collo S, Bartels DH, Bell ML, Benjamin EJ, Bennett D, Bhalla K, Bikbov B, Bin Abdulhak A, Birbeck G, Blyth F, Bolliger I, Boufous S, Bucello C, Burch M, Burney P, Carapetis J, Chen H, Chou D, Chugh SS, Coffeng LE, Colan SD, Colquhoun S, Colson KE, Condon J, Connor MD, Cooper LT, Corriere M, Cortinovis M, de Vaccaro KC, Couser W, Cowie BC, Criqui MH, Cross M, Dabhadkar KC, Dahodwala N, De Leo D, Degenhardt L, Delossantos A, Denenberg J, Des Jarlais DC, Dharmaratne SD, Dorsey ER, Driscoll T, Duber H, Ebel B, Erwin PJ, Espindola P, Ezzati M, Feigin V, Flaxman AD, Forouzanfar MH, Fowkes FG, Franklin R, Fransen M, Freeman MK, Gabriel SE, Gakidou E, Gaspari F, Gillum RF, Gonzalez-Medina D, Halasa YA, Haring D, Harrison JE, Havmoeller R, Hay RJ, Hoen B, Hotez PJ, Hoy D, Jacobsen KH, James SL, Jasrasaria R, Jayaraman S, Johns N, Karthikeyan G, Kassebaum N, Keren A, Khoo JP, Knowlton LM, Kobusingye O, Koranteng A, Krishnamurthi R, Lipnick M, Lipshultz SE, Ohno SL, Mabweijano J, MacIntyre MF, Mallinger L, March L, Marks GB, Marks R, Matsumori A, Matzopoulos R, Mayosi BM, McAnulty JH, McDermott MM, McGrath J, Mensah GA, Merriman TR, Michaud C, Miller M, Miller TR, Mock C, Mocumbi AO, Mokdad AA, Moran A, Mulholland K, Nair MN, Naldi L, Narayan KM, Nasseri K, Norman P, O'Donnell M, Omer SB, Ortblad K, Osborne R, Ozgediz D, Pahari B, Pandian JD, Rivero AP, Padilla RP, Perez-Ruiz F, Perico N, Phillips D, Pierce K, Pope CA, 3rd, Porrini E, Pourmalek F, Raju M, Ranganathan D, Rehm JT, Rein DB, Remuzzi G, Rivara FP, Roberts T, De Leon FR, Rosenfeld LC, Rushton L, Sacco RL, Salomon JA, Sampson U, Sanman E, Schwebel DC, Segui-Gomez M, Shepard DS, Singh D, Singleton J, Sliwa K, Smith E, Steer A, Taylor JA, Thomas B, Tleyjeh IM, Towbin JA, Truelsen T, Undurraga EA, Venketasubramanian N, Vijayakumar L, Vos T, Wagner GR, Wang M, Wang W, Watt K, Weinstock MA, Weintraub R, Wilkinson JD, Woolf AD, Wulf S, Yeh PH, Yip P, Zabetian A, Zheng ZJ, Lopez AD, Murray CJ, AlMazroa MA, Memish ZA: Global and regional mortality from 235 causes of death for 20 age groups in 1990 and 2010: a systematic analysis for the Global Burden of Disease Study 2010. Lancet 2012;380:2095-2128.

2 Xue C, Hu Z, Jiang W, Zhao Y, Xu F, Huang Y, Zhao H, Wu J, Zhang Y, Zhao L, Zhang J, Chen L, Zhang L: National survey of the medical treatment status for non-small cell lung cancer (NSCLC) in China. Lung Cancer 2012;77:371-375.

3 Wang Y, Gu J, Roth JA, Hildebrandt MA, Lippman SM, Ye Y, Minna JD, Wu X: Pathway-based serum microRNA profiling and survival in patients with advanced stage non-small cell lung cancer. Cancer Res 2013;73:4801-4809.

4 Dela Cruz CS, Tanoue LT, Matthay RA: Lung cancer: epidemiology, etiology, and prevention. Clin Chest Med 2011;32:605-644.

5 Tang S, Pan Y, Wang Y, Hu L, Cao S, Chu M, Dai J, Shu Y, Xu L, Chen J, Jin G, Hu Z, Ma H, Shen H: Genome-wide association study of survival in early-stage non-small cell lung cancer. Ann Surg Oncol 2015;22:630-635.

6 Xu YH, Lu S: A meta-analysis of STAT3 and phospho-STAT3 expression and survival of patients with non-small-cell lung cancer. Eur J Surg Oncol 2014;40:311-317.

7 Morgensztern D, Ng SH, Gao F, Govindan R: Trends in stage distribution for patients with non-small cell lung cancer: a National Cancer Database survey. J Thorac Oncol 2010;5:29-33.

8 Sequist LV, Martins RG, Spigel D, Grunberg SM, Spira A, Janne PA, Joshi VA, McCollum D, Evans TL, Muzikansky A, Kuhlmann GL, Han M, Goldberg JS, Settleman J, Iafrate AJ, Engelman JA, Haber DA, Johnson BE, Lynch TJ: First-line gefitinib in patients with advanced non-small-cell lung cancer harboring somatic EGFR mutations. J Clin Oncol 2008;26:2442-2449.

9 Xiong S, Zheng Y, Jiang P, Liu R, Liu X, Chu Y: MicroRNA-7 inhibits the growth of human non-small cell lung cancer A549 cells through targeting BCL-2. Int J Biol Sci 2011;7:805-814.

10 Zhang B, Liu T, Wu T, Wang Z, Rao Z, Gao J: microRNA-137 functions as a tumor suppressor in human non-small cell lung cancer by targeting SLC22A18. Int J Biol Macromol 2015;74:111-118.

11 Wang S, Su X, Bai H, Zhao J, Duan J, An T, Zhuo M, Wang Z, Wu M, Li Z, Zhu J, Wang J: Identification of plasma microRNA profiles for primary resistance to EGFR-TKIs in advanced non-small cell lung cancer (NSCLC) patients with EGFR activating mutation. J Hematol Oncol 2015;8:127.
12 Zhou H, Guo W, Zhao Y, Wang Y, Zha R, Ding J, Liang L, Yang G, Chen Z, Ma B, Yin B: MicroRNA-135a acts as a putative tumor suppressor by directly targeting very low density lipoprotein receptor in human gallbladder cancer. Cancer Sci 2014;105:956-965.
13 Kroiss A, Vincent S, Decaussin-Petrucci M, Meugnier E, Viallet J, Ruffion A, Chalmel F, Samarut J, Allioli N: Androgen-regulated microRNA-135a decreases prostate cancer cell migration and invasion through downregulating ROCK1 and ROCK2. Oncogene 2015;34:2846-2855.
14 Wu H, Huang M, Cao P, Wang T, Shu Y, Liu P: MiR-135a targets JAK2 and inhibits gastric cancer cell proliferation. Cancer Biol Ther 2012;13:281-288.
15 Zhang YK, Sun B, Sui G: Serum microRNA-135a downregulation as a prognostic marker of non-small cell lung cancer. Genet Mol Res 2016;15:
16 Yamada Y, Hidaka H, Seki N, Yoshino H, Yamasaki T, Itesako T, Nakagawa M, Enokida H: Tumor-suppressive microRNA-135a inhibits cancer cell proliferation by targeting the c-MYC oncogene in renal cell carcinoma. Cancer Sci 2013;104:304-312.
17 Navarro A, Diaz T, Martinez A, Gaya A, Pons A, Gel B, Codony C, Ferrer G, Martinez C, Montserrat E, Monzo M: Regulation of JAK2 by miR-135a: prognostic impact in classic Hodgkin lymphoma. Blood 2009;114:2945-2951.
18 Shin JY, Kim YI, Cho SJ, Lee MK, Kook MC, Lee JH, Lee SS, Ashktorab H, Smoot DT, Ryu KW, Kim YW, Choi IJ: MicroRNA 135a suppresses lymph node metastasis through down-regulation of ROCK1 in early gastric cancer. PLoS One 2014;9:e85205.
19 Chen M, Du Y, Qui M, Wang M, Chen K, Huang Z, Jiang M, Xiong F, Chen J, Zhou J, Jiang F, Yin L, Tang Y, Ye L, Zhan Z, Duan J, Fu H, Zhang X: Ophiopogonin B-induced autophagy in non-small cell lung cancer cells via inhibition of the PI3K/Akt signaling pathway. Oncol Rep 2013;29:430-436.
20 Zhen Y, Li D, Li W, Yao W, Wu A, Huang J, Gu H, Huang Y, Wang Y, Wu J, Chen M, Wu D, Lyu Q, Fang W, Wu B: Reduced PDCD4 Expression Promotes Cell Growth Through PI3K/Akt Signaling in Non-Small Cell Lung Cancer. Oncol Res 2016;23:61-68.
21 Ma J, Sawai H, Matsuo Y, Ochi N, Yasuda A, Takahashi H, Wakasugi T, Funahashi H, Sato M, Takeyama H: IGF-1 mediates PTEN suppression and enhances cell invasion and proliferation via activation of the IGF-1/PI3K/Akt signaling pathway in pancreatic cancer cells. J Surg Res 2010;160:90-101.
22 Salani B, Maffioli S, Hamoudane M, Parodi A, Ravera S, Passalacqua M, Alama A, Nhiri M, Cordera R, Maggi D: Caveolin-1 is essential for metformin inhibitory effect on IGF1 action in non-small-cell lung cancer cells. FASEB J 2012;26:788-798.
23 Gibbs AR, Thunnissen FB: Histological typing of lung and pleural tumours: third edition. J Clin Pathol 2001;54:498-499.
24 Rami-Porta R, Crowley JJ, Goldstraw P: The revised TNM staging system for lung cancer. Ann Thorac Cardiovasc Surg 2009;15:4-9.
25 Ma Y, Ma L, Guo Q, Zhang S: Expression of bone morphogenetic protein-2 and its receptors in epithelial ovarian cancer and their influence on the prognosis of ovarian cancer patients. J Exp Clin Cancer Res 2010;29:85.
26 Weidner N, Carroll PR, Flax J, Blumenfeld W, Folkman J: Tumor angiogenesis correlates with metastasis in invasive prostate carcinoma. Am J Pathol 1993;143:401-409.
27 Tuo YL, Li XM, Luo J: Long noncoding RNA UCA1 modulates breast cancer cell growth and apoptosis through decreasing tumor suppressive miR-143. Eur Rev Med Pharmacol Sci 2015;19:3403-3411.
28 Wu S, Lin Y, Xu D, Chen J, Shu M, Zhou Y, Zhu W, Su X, Zhou Y, Qiu P, Yan G: MiR-135a functions as a selective killer of malignant glioma. Oncogene 2012;31:3866-3874.
29 Cui X, Zhang L, Luo J, Rajasekaran A, Hazra S, Cacalano N, Dubinett SM: Unphosphorylated STAT6 contributes to constitutive cyclooxygenase-2 expression in human non-small cell lung cancer. Oncogene 2007;26:4253-4260.
30 Shi H, Ji Y, Zhang D, Liu Y, Fang P: MiR-135a inhibits migration and invasion and regulates EMT-related marker genes by targeting KLF8 in lung cancer cells. Biochem Biophys Res Commun 2015;465:125-130.

31 Wu DW, Hsu NY, Wang YC, Lee MC, Cheng YW, Chen CY, Lee H: c-Myc suppresses microRNA-29b to promote tumor aggressiveness and poor outcomes in non-small cell lung cancer by targeting FHIT. Oncogene 2015;34:2072-2082.
32 Zhao M, Gao FH, Wang JY, Liu F, Yuan HH, Zhang WY, Jiang B: JAK2/STAT3 signaling pathway activation mediates tumor angiogenesis by upregulation of VEGF and bFGF in non-small-cell lung cancer. Lung Cancer 2011;73:366-374.
33 Vigil D, Kim TY, Plachco A, Garton AJ, Castaldo L, Pachter JA, Dong H, Chen X, Tokar B, Campbell SL, Der CJ: ROCK1 and ROCK2 are required for non-small cell lung cancer anchorage-independent growth and invasion. Cancer Res 2012;72:5338-5347.
34 Kim JS, Kim ES, Liu D, Lee JJ, Solis L, Behrens C, Lippman SM, Hong WK, Wistuba, II, Lee HY: Prognostic implications of tumoral expression of insulin like growth factors 1 and 2 in patients with non-small-cell lung cancer. Clin Lung Cancer 2014;15:213-221.
35 Liu CH, Bao HG, Ge YL, Wang SK, Shen Y, Xu L: Celecoxib inhibits insulin-like growth factor 1 induced growth and invasion in non-small cell lung cancer. Oncol Lett 2013;5:1943-1947.
36 Masago K, Fujita S, Togashi Y, Kim YH, Hatachi Y, Fukuhara A, Nagai H, Irisa K, Sakamori Y, Mio T, Mishima M: Clinical significance of epidermal growth factor receptor mutations and insulin-like growth factor 1 and its binding protein 3 in advanced non-squamous non-small cell lung cancer. Oncol Rep 2011;26:795-803.
37 Ge P, Cui Y, Liu F, Luan J, Zhou X, Han J: L-carnitine affects osteoblast differentiation in NIH3T3 fibroblasts by the IGF-1/PI3K/Akt signalling pathway. Biosci Trends 2015;9:42-48.
38 Nor JE, Christensen J, Mooney DJ, Polverini PJ: Vascular endothelial growth factor (VEGF)-mediated angiogenesis is associated with enhanced endothelial cell survival and induction of Bcl-2 expression. Am J Pathol 1999;154:375-384.
39 Zhang Q, Lao X, Huang J, Zhu Z, Pang L, Tang Y, Song Q, Huang J, Deng J, Deng N, Yang Q, Sengupta AM, Xiong L: Soluble production and function of vascular endothelial growth factor/basic fibroblast growth factor complex peptide. Biotechnol Prog 2015;31:194-203.
40 Shi J, Wei PK: Interleukin-8: A potent promoter of angiogenesis in gastric cancer. Oncol Lett 2016;11:1043-1050.
41 Li X, Feng Y, Liu J, Feng X, Zhou K, Tang X: Epigallocatechin-3-gallate inhibits IGF-I-stimulated lung cancer angiogenesis through downregulation of HIF-1alpha and VEGF expression. J Nutrigenet Nutrigenomics 2013;6:169-178.
42 Ma J, Sawai H, Ochi N, Matsuo Y, Xu D, Yasuda A, Takahashi H, Wakasugi T, Takeyama H: PTEN regulates angiogenesis through PI3K/Akt/VEGF signaling pathway in human pancreatic cancer cells. Mol Cell Biochem 2009;331:161-171.